NASA/TM—2019-220383

Near-Exit Pressure Fluctuations in Jets From Circular and Rectangular Nozzles

K.B.M.Q. Zaman and A.F. Fagan
Glenn Research Center, Cleveland, Ohio

November 2019

NASA STI Program . . . in Profile

Since its founding, NASA has been dedicated to the advancement of aeronautics and space science. The NASA Scientific and Technical Information (STI) Program plays a key part in helping NASA maintain this important role.

The NASA STI Program operates under the auspices of the Agency Chief Information Officer. It collects, organizes, provides for archiving, and disseminates NASA's STI. The NASA STI Program provides access to the NASA Technical Report Server—Registered (NTRS Reg) and NASA Technical Report Server—Public (NTRS) thus providing one of the largest collections of aeronautical and space science STI in the world. Results are published in both non-NASA channels and by NASA in the NASA STI Report Series, which includes the following report types:

- TECHNICAL PUBLICATION. Reports of completed research or a major significant phase of research that present the results of NASA programs and include extensive data or theoretical analysis. Includes compilations of significant scientific and technical data and information deemed to be of continuing reference value. NASA counter-part of peer-reviewed formal professional papers, but has less stringent limitations on manuscript length and extent of graphic presentations.

- TECHNICAL MEMORANDUM. Scientific and technical findings that are preliminary or of specialized interest, e.g., "quick-release" reports, working papers, and bibliographies that contain minimal annotation. Does not contain extensive analysis.

- CONTRACTOR REPORT. Scientific and technical findings by NASA-sponsored contractors and grantees.

- CONFERENCE PUBLICATION. Collected papers from scientific and technical conferences, symposia, seminars, or other meetings sponsored or co-sponsored by NASA.

- SPECIAL PUBLICATION. Scientific, technical, or historical information from NASA programs, projects, and missions, often concerned with subjects having substantial public interest.

- TECHNICAL TRANSLATION. English-language translations of foreign scientific and technical material pertinent to NASA's mission.

For more information about the NASA STI program, see the following:

- Access the NASA STI program home page at http://www.sti.nasa.gov

- E-mail your question to help@sti.nasa.gov

- Fax your question to the NASA STI Information Desk at 757-864-6500

- Telephone the NASA STI Information Desk at 757-864-9658

- Write to:
  NASA STI Program
  Mail Stop 148
  NASA Langley Research Center
  Hampton, VA 23681-2199

NASA/TM—2019-220383

Near-Exit Pressure Fluctuations in Jets From Circular and Rectangular Nozzles

K.B.M.Q. Zaman and A.F. Fagan
Glenn Research Center, Cleveland, Ohio

National Aeronautics and
Space Administration

Glenn Research Center
Cleveland, Ohio 44135

November 2019

Acknowledgments

The first author wishes to thank Prof. Aaron Towne of University of Michigan for a discussion of the topic at the AIAA/CEAS Aeroacoustics Meeting in May, 2019 that inspired the present experimental effort. Thanks are also due to Prof. Christopher Tam of Florida State University whose analytical work inspired the experiments with the rectangular nozzles, and to Dr. Puja Upadhyay for help in various forms throughout the study. This work is supported by NASA's Commercial Supersonic Technologies (CST) and Transformational Tools and Technologies (TTT) Projects.

Available from

NASA STI Program
Mail Stop 148
NASA Langley Research Center
Hampton, VA 23681-2199

National Technical Information Service
5285 Port Royal Road
Springfield, VA 22161
703-605-6000

This report is available in electronic form at http://www.sti.nasa.gov/ and http://ntrs.nasa.gov/

Near-Exit Pressure Fluctuations in Jets From Circular and Rectangular Nozzles

K.B.M.Q. Zaman and A.F. Fagan
National Aeronautics and Space Administration
Glenn Research Center
Cleveland, Ohio 44135

Abstract

This article documents some experimental observations made for near-exit unsteady pressure fluctuations in high-speed jets. These fluctuations are apparently related to 'trapped waves' within the jet potential core as investigated and reported recently by other researchers. Round nozzles of three different diameters and rectangular nozzles of three different aspect ratios are studied. The pressure fluctuations manifest as a series of peaks in the spectra. These 'trapped wave spectral peaks' are found with all nozzles. Their characteristics and variations with axial and radial distances as well as with jet Mach number are documented. Effects of initial boundary layer state and the presence of a surface nearby as well as the scaling of the frequencies of the spectral peaks are studied and discussed.

Introduction

Recent research based on 'mining' of data from a Large Eddy Simulation (LES) has identified a system of instability waves in round high-subsonic jets that are not the same as the well-known Kelvin-Helmholtz (K-H) waves. These, often referred to as 'trapped waves', are apparently predicted by a second-branch solution of spatial stability theory for free shear layers. Reference 1 provides a seminal account of the phenomenon. These waves are not detectable in the far-field and hence went unnoticed in the vast literature on jet noise experiments. They have also gone undetected in the vast literature on jet instability and excitation studies apparently because the K-H waves grow fast and dominate the flowfield. It is also possible that probe interference such as with hot-wire anemometry alters the trapped waves and renders them difficult to discern.

However, a microphone placed close to the nozzle exit and just outside the shear layer apparently picks up the signature of these waves. Reference 2 is perhaps the first experimental study observing such pressure fluctuations near the edge of a jet. A few of the microphones in a 'phased array' exhibited certain spectral peaks. The authors thought these were spurious and possibly related to facility resonances. They explored the connection of these peaks to upstream duct modes and the results were inconclusive. They narrated their observations in an appendix of the paper. It should be noted that the authors of Reference 1 also conducted an experiment and observed similar spectral peaks whose frequencies compared well with their LES as well as analytical results.

Clearly, there should be an academic interest to understand these waves. They are an integral part of jet shear layer instability that in turn dictates the initial development of the jet. Even though these waves are not readily detectable in the far field, it stands to reason that computational fluid dynamics and aero acoustics (CFD and CAA) codes must account for them for accurate prediction of jet noise. A significant practical relevance could be in jet-surface interaction and, therefore, in propulsion/airframe noise. As it will be shown, a plate placed near a rectangular as well as a round nozzle is found to amplify these spectral peaks and sometimes yield resonant tones apparently locking to one of those peaks.

The present experimental study is undertaken to explore further details of the unsteady pressure fluctuations near the nozzle exit. Following Reference 1, such fluctuations are simply referred to as 'trapped waves' and the corresponding spectral peaks in the pressure signal as 'trapped wave spectral peaks'. Using a single microphone the pressure spectra are measured for varying streamwise and radial distances as well as for varying jet Mach number. This is carried out for round nozzles of different diameters as well as for rectangular nozzles of different aspect ratios. The effects of the exit boundary layer state as well as disturbances introduced by tabs on the spectral peaks are studied. The results obtained so far are limited and more exploration is called for in the future. However, the data may be of sufficient interest to researchers working in this relatively new area especially to those carrying out numerical and analytical studies. Hence a documentation of the results is deemed worthwhile for fast dissemination, and that is the objective of this technical memorandum. In it, we describe key findings and make observations simply from an experimentalist's vantage point without any attempt to relate them to results, e.g., discussed in Reference 1.

Experimental Facility

The experiments are conducted in an open jet facility at the NASA Glenn Research Center (GRC). Compressed air passes through a 30 in. diameter plenum chamber before exhausting through the nozzle into the ambient of the test chamber. An interested reader may find further description of the facility in earlier publications, e.g., (Ref. 3). The pressure fluctuation spectra are measured by a microphone (1/4-in., B&K 4135) mounted on a probe traversing mechanism. All spectral data presented in the following are taken with the 1/4-in. microphone. Since a protection grid normally used with the microphone can sometimes produce spurious high frequency noise, all data are obtained with having it removed. As described with the results, for spatial resolution concerns a 1/8-in. microphone is also used to repeat some data with a small nozzle. Limited far-field noise data, taken with a fixed microphone, are discussed. Data acquisition is done using a National Instruments A/D card and LabVIEW™ software. Spectral analysis is done typically over 0 to 50 kHz with a bandwidth of 50 Hz, using a data rate of 100 kHz and a 50 kHz low-pass filter. For larger nozzles the analysis range is sometimes reduced with a correspondingly shorter bandwidth, so that the spectral peaks are captured with adequate resolution.

Figure 1 shows pictures of various nozzle configurations. All nozzles are convergent. The one in Figure 1(a) is the 'SMC000' case (small metallic chevron nozzle; without chevrons) that will be referred to simply as 'SMC' in the following. It is attached to the plenum chamber through adapters having smooth, converging interior contours. This round nozzle with exit diameter of 2 in. has been used previously in several experimental as well as numerical studies; Reference 4 cites a few such previous and ongoing works. All dimensions are given in inches.

The configuration shown in Figure 1(b) involves the SMC nozzle with a 12 in. long upstream pipe. It has been shown to generate a fully turbulent exit boundary layer whereas without the pipe the nozzle has a 'nominally laminar' boundary layer (Ref. 4). One set of data is obtained with two triangular tabs attached to the SMC nozzle, as shown in Figure 1(c). Each tab has equilateral triangular shape, with a base width of 0.2 in., and penetrate the flow at 45°. Figure 1(d) and (e) show a 1 in. and 0.58 in. diameter round nozzle, respectively. While the exit boundary layers for the smaller nozzles have not been measured they are also likely to be nominally laminar. Figure 1(f) shows a 2:1 aspect ratio rectangular nozzle with the long edge placed horizontally. Figure 1(g) shows an 8:1 aspect ratio nozzle with the long edge placed vertically. In most of the pictures the microphone used for the measurements can be seen. Not shown is a 4:1 rectangular nozzle, also used in the experiment. All three rectangular cases have an equivalent diameter of 2.12 in. based on the exit area; further descriptions including exit boundary layer data can be found in Reference 5. The last case shown in Figure 1(h) is the SMC nozzle together with a rectangular plate placed underneath; the purpose and the geometry will be described with the results.

(a) 

(b) 

(c) 

(d) 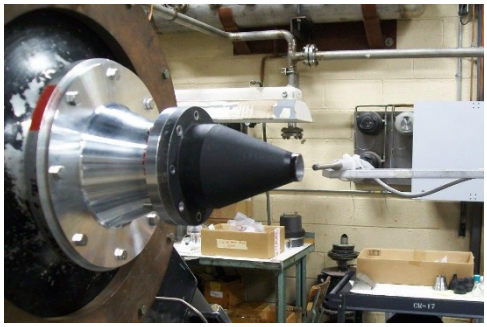

(e) 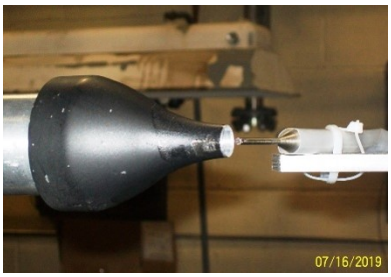

(f) 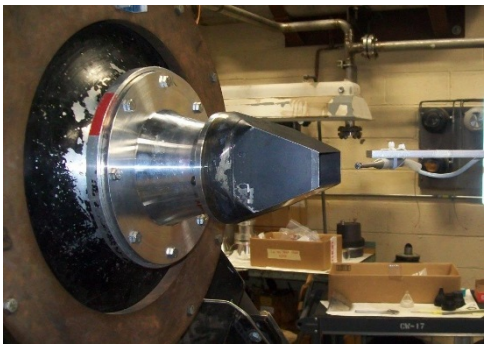

(g) 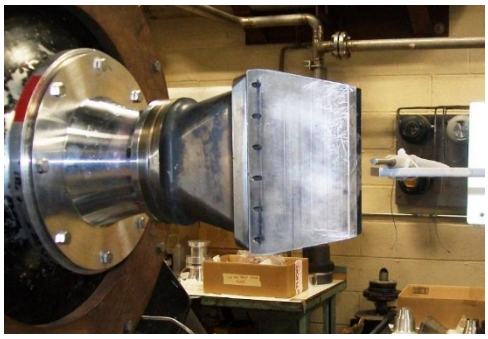

(h) 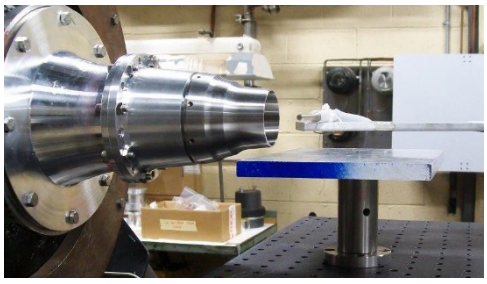

Figure 1.—Nozzle configurations. (a) D = 2 in. ('SMC') nozzle, (b) SMC nozzle with an upstream pipe, (c) SMC nozzle with 2 tabs, (d) D = 1 in. nozzle, (e) D = 0.58 in. nozzle, (f) 2:1 rectangular nozzle, (g) 8:1 rectangular nozzle, (h) SMC nozzle with a flat plate underneath.

The 'jet Mach number' M_J is used as an independent variable. It is defined based on the plenum pressure, p_0, and the ambient pressure, p_a, and given by, $M_J = \left(\left((p_0/p_a)^{(\gamma-1)/\gamma} - 1 \right) \frac{2}{\gamma - 1} \right) 1/2$, where γ is the ratio of specific heats for air. Note that in supersonic conditions, it is fictitious and represents the Mach number had the flow expanded fully. All data reported are for cold flows, i.e., with the total temperature the same everywhere as in the ambient.

Results and Discussion

Round Nozzle Data

Pressure fluctuation spectra measured near the exit of the SMC nozzle are shown in Figure 2(a) for varying streamwise distance (x) with a fixed radial distance (r = 0.75); here, the distances are nondimensionalized by the nozzle diameter (2 in.). The coordinate origin is located at the center of the nozzle exit. The ordinate in Figure 2(a) pertains to the trace at the bottom (x = 0) and successive traces are staggered by 10 dB. A series of peaks mark the spectra especially near the nozzle exit for the given r. These are similar to those reported in References 1 and 2. Away from the exit the spectral peaks get buried under broadband turbulence apparently when the microphone begins to encounter some flow. In Figure 2(b) corresponding data are shown for a fixed x but for varying r. When the microphone is too close to the jet (r = 0.6), it encounters flow resulting in a broadband peak, in this case, centered around 12 kHz. The spectral peaks are seen to diminish in amplitude with increasing radial distance.

Corresponding data for varying jet Mach number (M_J) at a point near the nozzle exit (x = 0.2, r = 0.75) are shown in Figure 3(a). The trapped wave spectral peaks are not clearly visible at the lowest M_J (= 0.548) but they become prominent with increasing M_J. The frequency of a given spectral peak decreases with increasing M_J. Such a behavior was also noted in Reference 2 leading to the inference that these peaks do not follow a Strouhal number scaling; (if the Strouhal number based on nozzle diameter remained constant, the frequencies would have increased with increasing M_J). This point is addressed further later. In Figure 3(b) corresponding sound pressure level spectra in the 'far-field' are shown; the

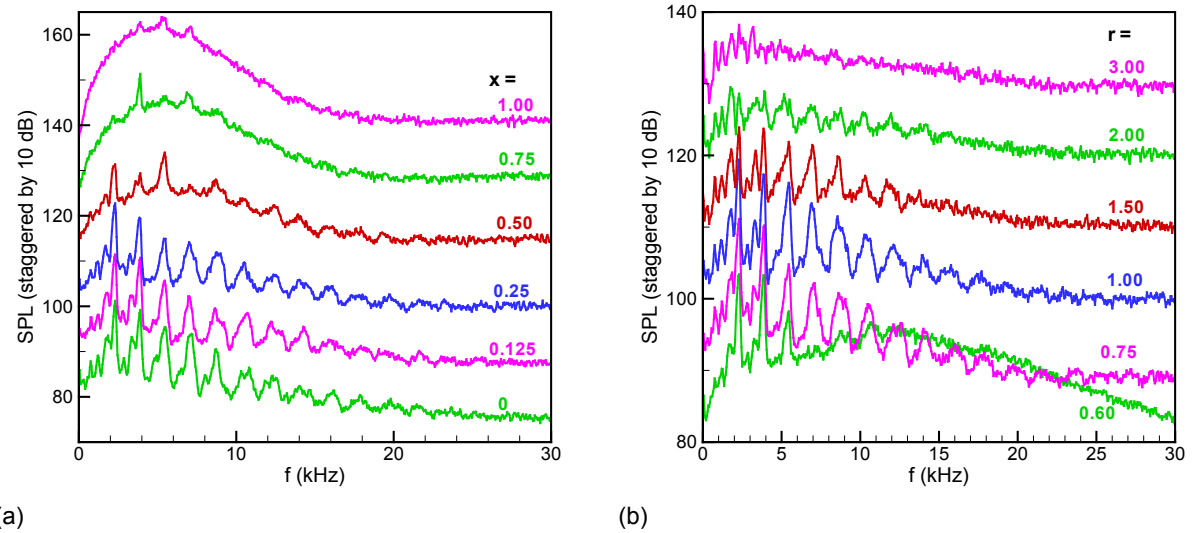

Figure 2.—Pressure spectra near the exit of the SMC (D = 2 in.) nozzle; M_J = 0.91. (a) Varying x at fixed r = 0.75, (b) varying r at fixed x = 0.2. (Distances normalized by D).

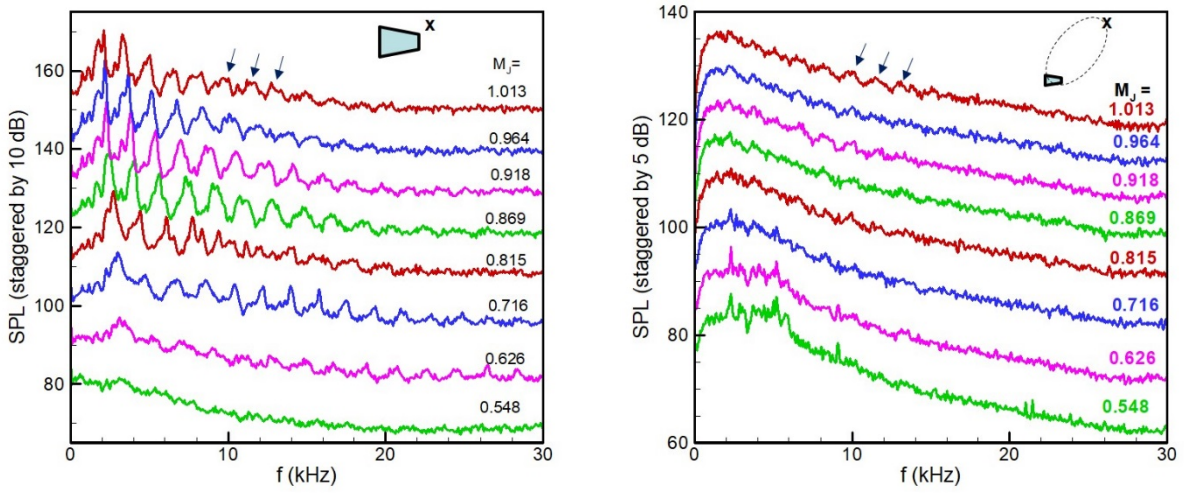

(a) (b)

Figure 3.—Pressure spectra near and far from the SMC nozzle with varying M_J. (a) Near-exit at x = 0.2, r = 0.75, (b) 25D away from the exit at 60° polar location relative to jet axis.

microphone location is 25D from the jet exit and at a polar angle of 60° relative to the jet axis (the location is shown schematically with inserts in some figures to aid the reader). The trapped wave spectral peaks are known to be undetectable in the far-field noise spectra. Here, some undulations (marked by the arrows) especially at higher M_J conditions can be noticed that appear to be the footprint of the trapped waves. It is possible this is because 25D distance is still not the far acoustic field, the test chamber is not anechoic, and there are some uncovered reflecting surfaces in the vicinity of the nozzle (e.g., the probe traversing mechanism, flanges etc.).

Figure 4 shows pairs of spectral data at three values of M_J. These data are for the SMC nozzle with one set taken with the upstream pipe (Figure 1(b)) and the other without the pipe (Figure 1(a)). Through hot-wire measurements it was shown earlier in Reference 4 that the nozzle with the pipe involves a fully turbulent exit boundary layer whereas the case without the pipe involves a ‘nominally laminar’ boundary layer. (In the latter case the mean velocity profile has a shape similar to that of a ‘Blasius-profile’ characteristic of laminar boundary layer but involves large fluctuation intensities. The former case involves a slow decay of mean velocity as the nozzle wall is approached with turbulent fluctuations penetrating far from the wall. The momentum thickness in the former case is at least three times larger than that in the latter case). The nearly congruent traces in each pair (Figure 4) indicate that the trapped waves are not influenced by the exit boundary layer (BL) characteristics. It is apparent that the trapped wave spectral peaks also do not scale on the exit BL thickness for a given boundary layer state (laminar or turbulent); BL thickness decreases with increasing M_J, so a Strouhal number based on the thickness would decrease more rapidly with increasing M_J. The frequency scaling is discussed further in the following. One other point is noteworthy. Figure 4 includes a set of data at a supersonic condition where screech has ensued (represented by the tall peak in the spectra which manifests as an audible tone). The progression of the spectral peaks with increasing M_J suggests that one of the trapped wave peaks has turned into the screech component. This point is also addressed further in the following.

Figure 5 shows pairs of spectra with and without two tabs attached to the SMC nozzle (Figure 1(c)). Tabs clearly affect the spectra with a large increase in broadband noise seen at the measurement point which is in close proximity of the jet. However, the trapped wave spectral peaks are not completely eliminated. Figure 6(a) shows data from the 1 in. diameter jet with varying x, similarly as done in Figure 2(a) for the 2 in. jet. Very similar trends are noted except that the frequencies of the peaks are

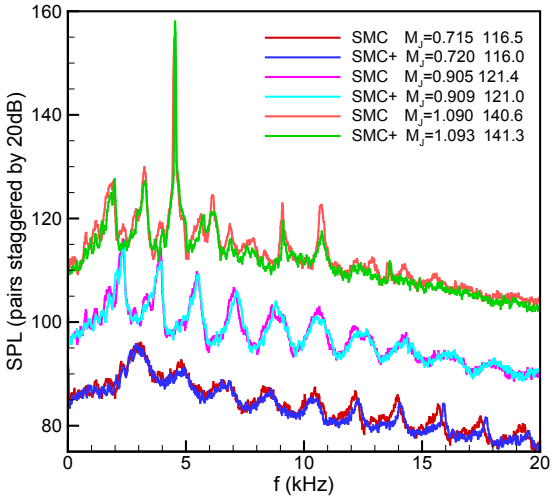

Figure 4.—Pressure spectra at x = 0.2 and r = 0.75 for the SMC nozzle with and without the upstream pipe. SMC+ denotes the pipe case (see Figure 1(b)).

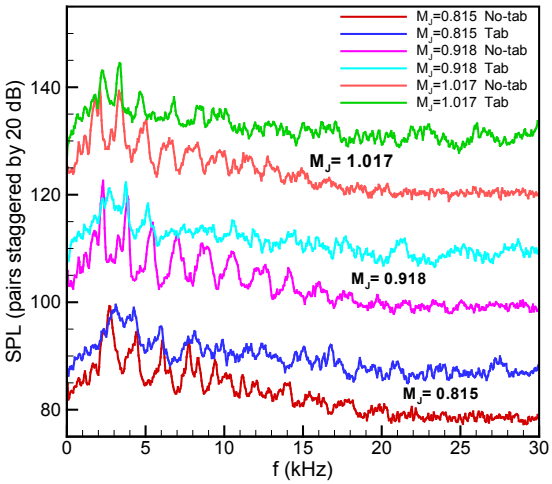

Figure 5.—Pressure spectra at x = 0.2 and r = 0.75 for the SMC nozzle with and without tabs (tab configuration shown in Figure 1(c)).

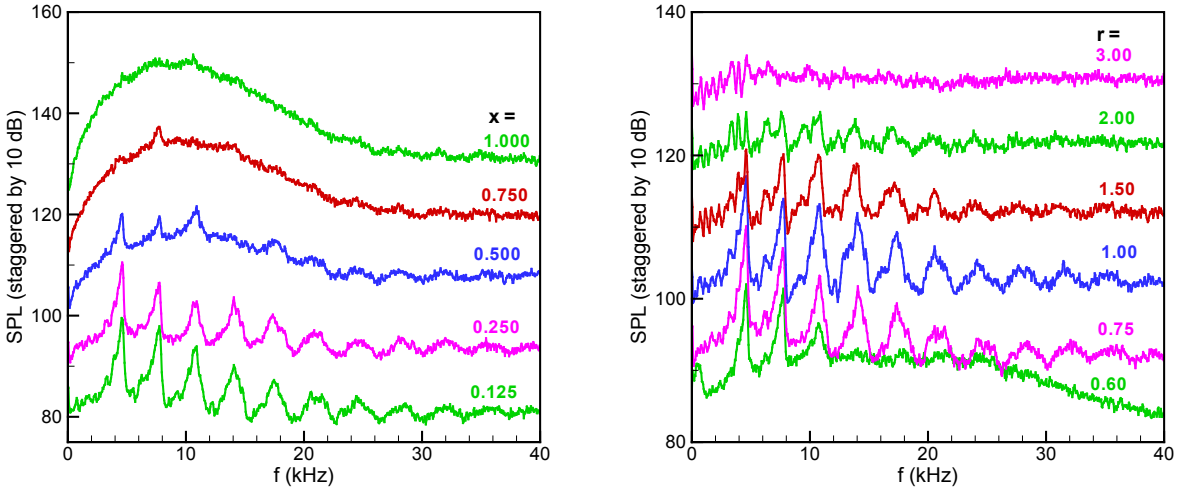

(a) (b)

Figure 6.—Pressure spectra near the exit of D = 1 in. nozzle for M_J = 0.91. (a) Varying x at fixed r = 0.75, (b) varying r at fixed x = 0.2.

higher; this is analyzed further shortly. The same comment can be made for radial variation of the spectra shown in Figure 6(b). Likewise, a similar trend is observed for jet Mach number variation, shown in Figure 7(a). In Figure 7(b) data for the 1 in. diameter nozzle are shown in the supersonic regime. In the range $M_J \geq 1.083$ there is screech. There is a stage jump around $M_J = 1.2$. An inspection again reveals a continuous trend. It is as if the screech component locks on to one of the trapped wave spectral peaks. With increasing M_J, it first locks on to the third peak (clearly at $M_J = 1.117$) and after the stage jump it locks on to the second peak. Throughout the entire M_J range covered, the frequency of an individual peak decreases with increasing M_J.

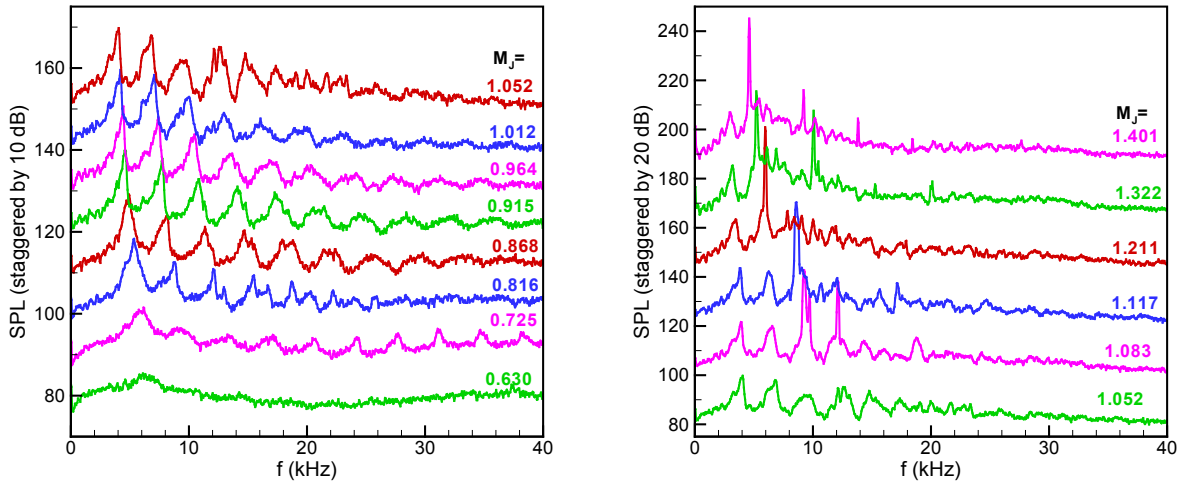

(a) (b)

Figure 7.—Pressure spectra for D = 1 in. jet with varying M_J; x = 0.2, r = 0.75. (a) Low Mach number range, (b) supersonic range.

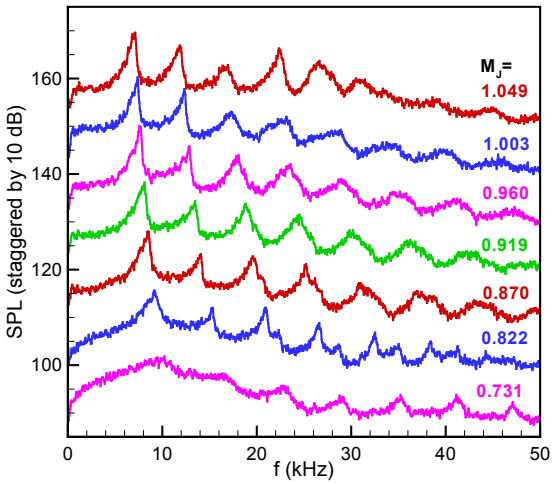

Figure 8.—Pressure spectra for D = 0.58 in. jet with varying M_J; x = 0.2, r = 0.75.

Data for the smallest (0.58 in. diameter) nozzle is shown only for variation of M_J, in Figure 8. These data are measured by the 1/4-in. microphone which is relatively large. A 1/8-in. microphone is used to cross-check and the spectral peaks are found to repeat well (not shown for brevity). Comparing the data in Figure 3(a), Figure 7(a), and Figure 8, a consistent increase in the frequencies of the trapped wave peaks is noted with decreasing nozzle diameter. This is examined in Figure 9 where data for all three nozzles are plotted as a function of Strouhal number based on the diameter; (jet velocity, defined to be equal to M_J times the ambient speed of sound, is used for velocity scale). Two sets of data are shown for M_J = 0.92 and 1.01, as examples, in Figure 9(a) and (b), respectively. The trapped wave spectral peaks are found to be approximately congruent for the three nozzles with different diameters. A scrutiny also reveals that the spectral peaks are not harmonics. For example, the first three peaks for M_J = 0.91 occur at Strouhal numbers 0.377, 0.624, and 0.879; those for M_J = 1.01 occur at 0.345, 0.576, and 0.808.

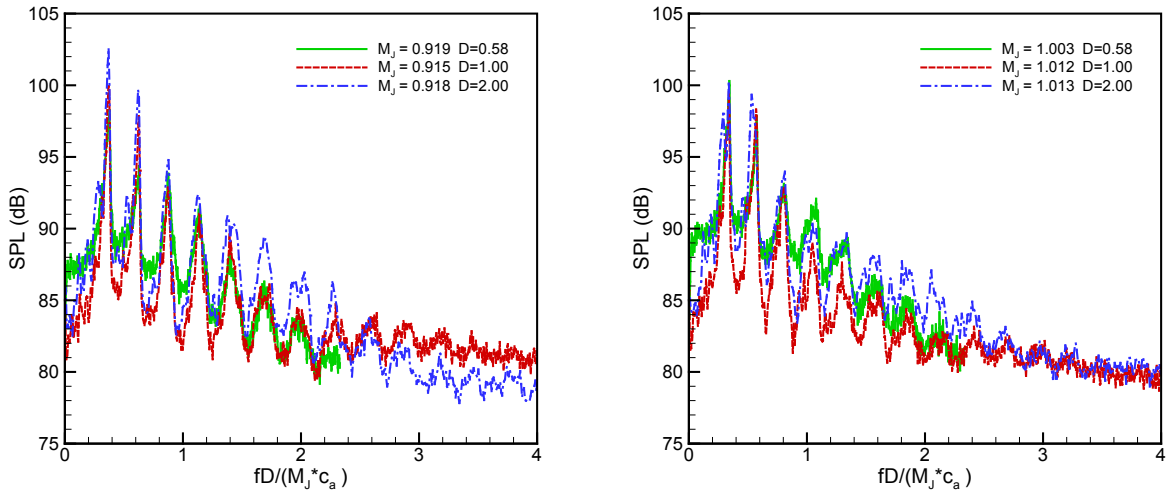

(a) (b)

Figure 9.—Pressure spectra for the three round nozzles shown as a function of Strouhal number based on diameter; $x = 0.2$, $r = 0.75$. (a) $M_J \approx 0.91$, (b) $M_J \approx 1.01$.

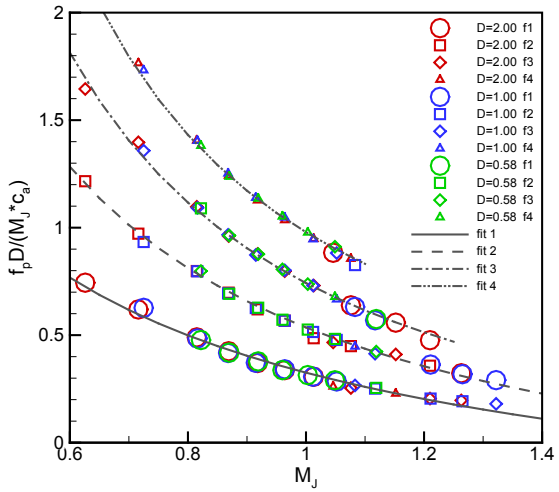

Figure 10.—Strouhal numbers of the four tallest spectral peaks, cross-plotted from data of Figure 3(a), Figure 7(a), and Figure 8 for the three round nozzle cases. Equations for fitted curves given in the text.

The Strouhal numbers of the four tallest peaks in each spectra (usually the four from the left at low frequencies) are plotted in Figure 10. The symbol size (and shape) are varied according to the amplitude; circles represent the highest while the square, diamond and delta shapes represent the lower amplitudes in decreasing order. An interesting trend emerges. The trapped wave spectral peaks follow distinct branches. Generally, the amplitudes are the highest at the lowest branch and decrease at the upper branches. However, screech, usually representing the tallest peak, often locks on to the peaks in the upper branches. Screech seems to blend with the family of curves quite well. This may lead one to speculate that the morphology of screech and the trapped waves trace to similar mechanisms; this, however, is a speculation at this time.

It is apparent that the trapped wave spectral peaks follow a Strouhal number scaling after all (based on nozzle diameter). However, the Strouhal number is not a constant and it is a distinct function of M_J in each of the branches. The data on exit BL effect (Figure 4) and for nozzles of different diameters (Figure 9 and Figure 10) strongly suggest that the spectral peaks do not scale on the initial shear layer (exit BL) thickness. Had the ratio of the thickness to diameter remained constant for all nozzles, scaling on the diameter would be equivalent to scaling on the exit BL thickness. Although it has not been measured, that ratio is unlikely to be the same for all three nozzles. Furthermore there is the stark contrast in BL state and thickness in Figure 4 that has negligible effect on the spectral peaks. In Figure 10 if the data were nondimensionalized by exit BL thickness instead of diameter they would not fall on a single curve for each branch. Thus, it is safe to infer that the trapped wave spectral peaks do not scale on initial shear layer thickness, contrasting the characteristics of K-H waves.

The data in Figure 10 provide an engineering correlation for prediction of the trapped wave frequencies for round nozzles. For a given diameter, the frequencies can be calculated using empirical curves fitted through each branch. Curves of the shape, $St = 1/M_J^{-A} + B$, are fitted where St is the Strouhal number (ordinate in Figure 10). The fitted curves are shown by the lines in Figure 10. The coefficients (A, B) for the four branches are as follows: (fit 1: 0.7169, –0.6745), (fit 2: 1.0926, –0.4642), (fit 3: 1.4260, –0.2578), and (fit 4: 1.6728, –0.0211).

Rectangular Nozzle Data

The data so far pertained to round nozzles. The behavior of near-exit pressure fluctuations were then explored for rectangular nozzles. The nozzles were readily available and the explorations could be extended with the same facility and instrumentation. With a rectangular nozzle the widths in the major and the minor axis directions present two length scales. The occurrence of the trapped waves is investigated on both the short and the long edges. Microphone locations nondimensionalized by the equivalent diameter (D_{eq} = 2.12 in.) are indicated in the captions of all following figures; coordinates y and z denote the vertical and horizontal distances from jet axis, respectively, while x denotes the axial distance from the nozzle exit.

Figure 11 shows the spectral traces with varying M_J for the 2:1 rectangular nozzle (exit: 1.328 by 2.665 in.) with the microphone placed on the major axis, i.e., near the short edge. For convenience, the microphone location is shown schematically with the insert. Obviously, the trapped waves are also detected with the rectangular nozzle! The trends are similar to that seen with round nozzles: they occur above a certain M_J and the frequencies decrease with increasing M_J. It will be shown next that the number of spectral peaks here depend on the side of the nozzle where the microphone is placed.

Data on the major axis versus the minor axis (short edge versus long edge) of the 2:1 case are compared in Figure 12(a) for M_J = 0.91. The trapped waves are also detected on the long edge, however, the peaks occur less frequently, coinciding approximately with every other peak seen on the short edge. Note that the microphone orientation relative to the edge of the nozzle is different for the two cases in Figure 12(a). That this did not cause a difference in the spectra is checked by another set of data taken with the nozzle rotated by 90°, shown in Figure 12(b). The difference in the number of trapped wave spectral peaks on the long and short edges are further documented in Figure 13 for two other values of M_J. The number of peaks seen on the long edge (minor axis) are approximately one-half of those seen on the short edge. The first (dominant) peak is seen on both edges but only the third and fifth seen on the short edge approximately coincide with the second and third seen on the long edge, respectively; at higher frequencies the amplitudes are small and there is increasing randomness in such matching.

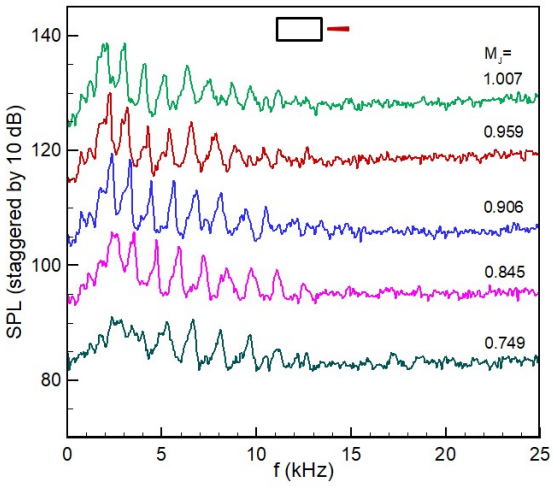

Figure 11.—Pressure spectra for the 2:1 aspect ratio rectangular nozzle with varying M_J; mic on short edge (major axis) at y = 0.943, z = 0 and x = 0.236. (Distances normalized by D_{eq} = 2.12 in.).

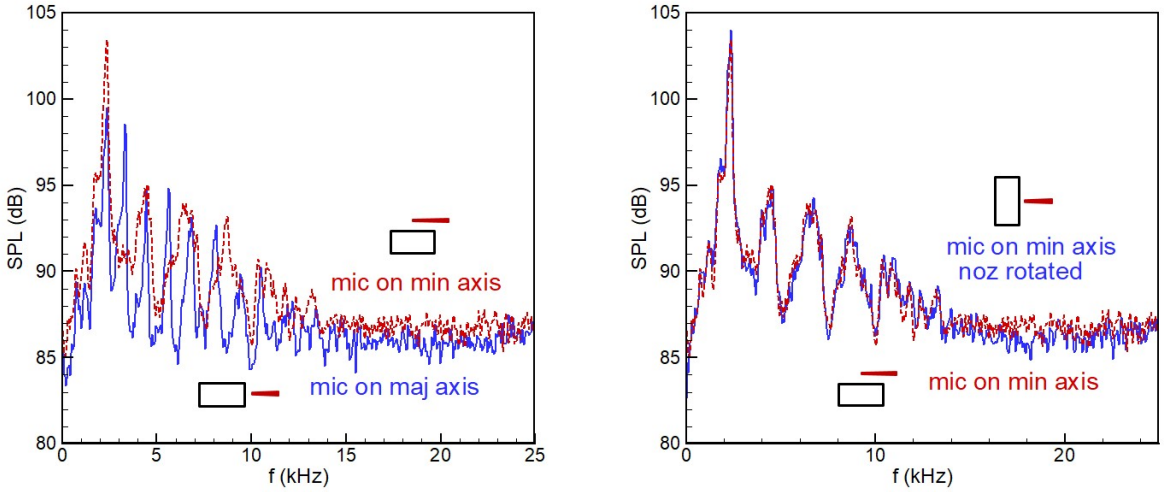

(a) (b)

Figure 12.—Pressure spectra for the 2:1 rectangular nozzle, M_J = 0.91, x = 0.236. (a) mic on long edge (minor axis) versus short edge (major axis), (b) data on short edge with two relative mic orientation. (Locations for 'Maj axis': y = 0.943, z = 0; 'min axis': y = 0, z = 0.637; 'min axis noz rotated': y = 0.637, z = 0.)

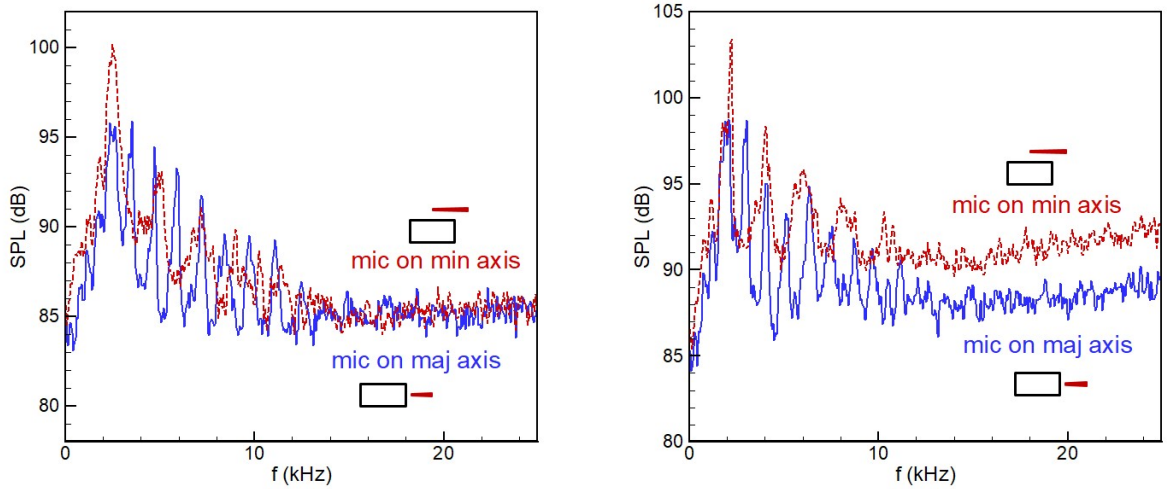

Figure 13.—Pressure spectra for the 2:1 rectangular nozzle with mic on short edge versus long edge for two other values of M_J (mic locations given in Figure 12 caption). (a) M_J = 0.845, (b) M_J = 1.007.

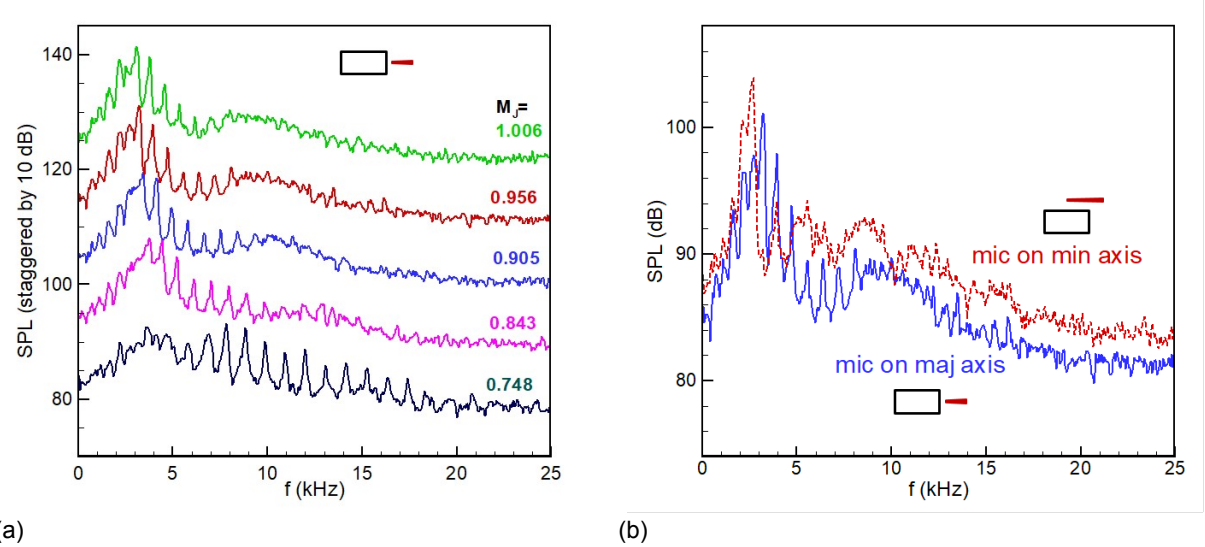

Figure 14.—Pressure spectra for the 4:1 aspect ratio rectangular nozzle, x = 0.189. (a) Varying M_J with mic on short edge (y = 1.108, z = 0); (b) for M_J = 0.91 with mic on short edge (y = 1.108, z = 0) versus long edge (y = 0, z = 0.443).

Corresponding data with varying M_J for the 4:1 aspect ratio case (exit: 0.940 by 3.765 in.) on the short edge are shown in Figure 14(a). The trapped wave peaks are again present, however, they are tightly packed. On the other hand, as shown in Figure 14(b), on the long edge the peaks are dispersed and not as sharp. An inspection suggests that the number of peaks on the long edge here are approximately 4 times less than those seen on the short edge.

The trend continues for the 8:1 aspect ratio nozzle (exit: 0.661 by 5.340 in.) as shown in Figure 15. On the short edge the peaks are more tightly spaced (Figure 15(a)). The number of peaks on the long edge appear to be approximately 8 times less than that seen on the short edge (Figure 15(b)). The long wavelengths (low frequency) noted on the long edge are not affected by microphone orientation (Figure 15(c)). The long waves are observed over the entire span and even near the corner of the nozzle (Figure 15(d)). Therefore, the ratio of the number of peaks seen on the long and short edges appear to be simply dictated by the aspect ratio. It is as if a lateral resonance in the major axis direction is detected on the minor axis location and vice versa.

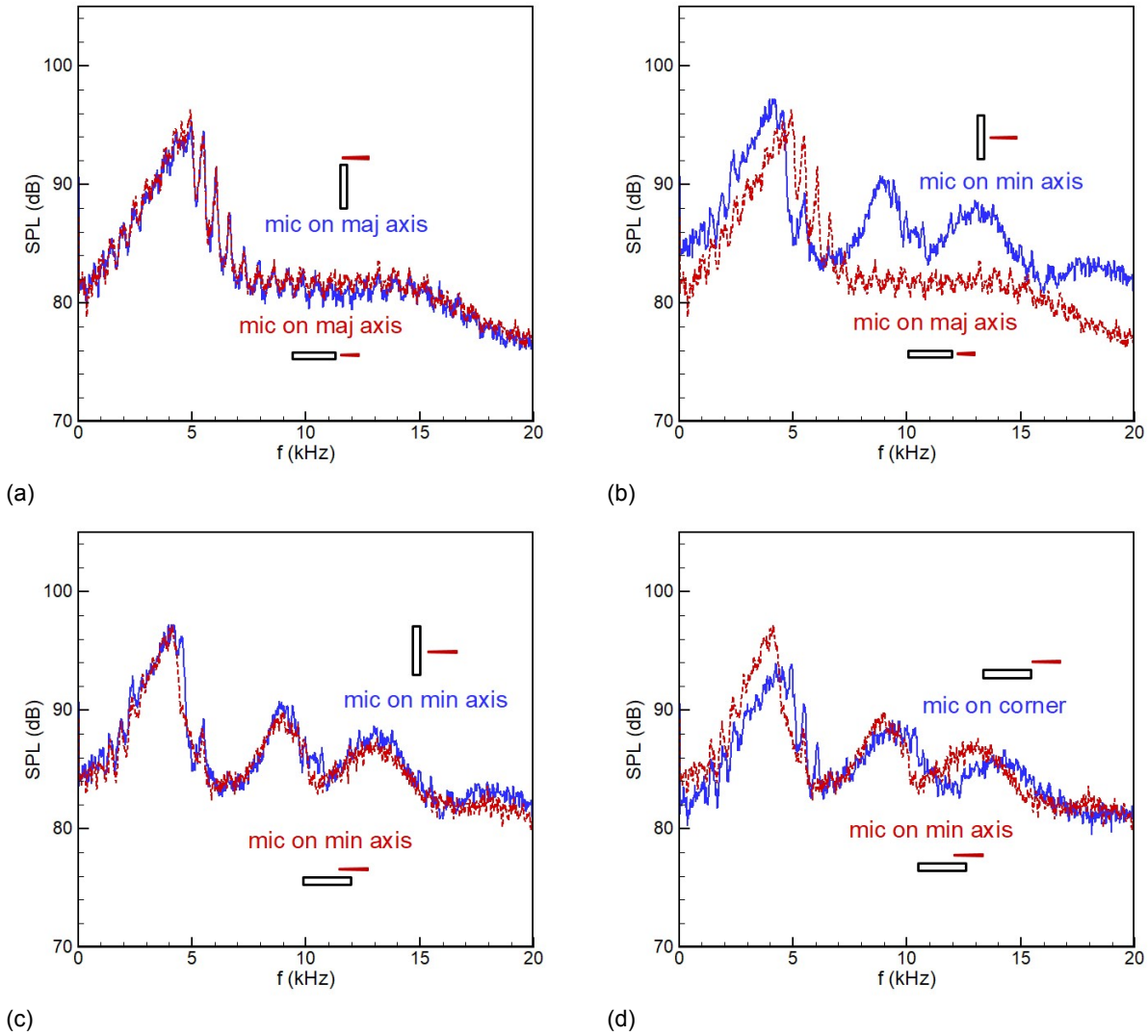

Figure 15.—Pressure spectra for the 8:1 aspect ratio rectangular nozzle at M_J = 0.91, x = 0.156. (a) Data on short edge with two mic orientation (y = 0, z = 1.42 and y = 1.42, z = 0); (b) data on short edge versus long edge (y = 0.31, z = 0 and y = 1.42, z = 0); (c) data on short edge with two mic orientation (y = 0.31, z = 0 and y = 0.63, z = 0.31); (d) data on short edge at two lateral locations (y = 1.26, z = 0.31 and y = 0.63, z = 0.31).

Jet-Surface Interaction

A practical significance of the trapped waves could be in jet-surface interaction and hence in propulsion-airframe noise. Note that with the same 8:1 rectangular nozzle a resonant tone was observed before when a flat surface was placed nearby; the phenomenon was studied and reported in Reference 3. Recently, an analysis of the occurrence of various spectral peaks (including the tone) for that flow was done in Reference 6. The analysis followed from Prof. Tam's earlier work addressing various aspects of shear layer instability, (see Ref. 1). Here, we further explore the resonance in light of the trapped wave spectral behavior noted and discussed in the foregoing.

First, the resonance phenomenon is reproduced with a plate placed just underneath the long edge of the nozzle. The spectral data with a schematic of the experimental arrangement are shown in Figure 16. Data for several values of M_J are shown in Figure 16(a). A resonant tone occurs around 1375 Hz. With increasing M_J, the tone ensues at a high subsonic condition and the frequency varies slightly with further increase in M_J. The data for $M_J = 0.91$ is now compared with corresponding data for the bare nozzle (no plate) in Figure 16(b). For the no-plate case, data on both the long and short edges are included. It is clear that the tone does not correspond to the trapped wave spectral peaks seen on the long edge (indicated by the red colored arrows). Although not quite clear it is possible that the tone coincides with one of the trapped wave peaks seen on the short edge (indicated by the vertical line and the blue colored arrow).

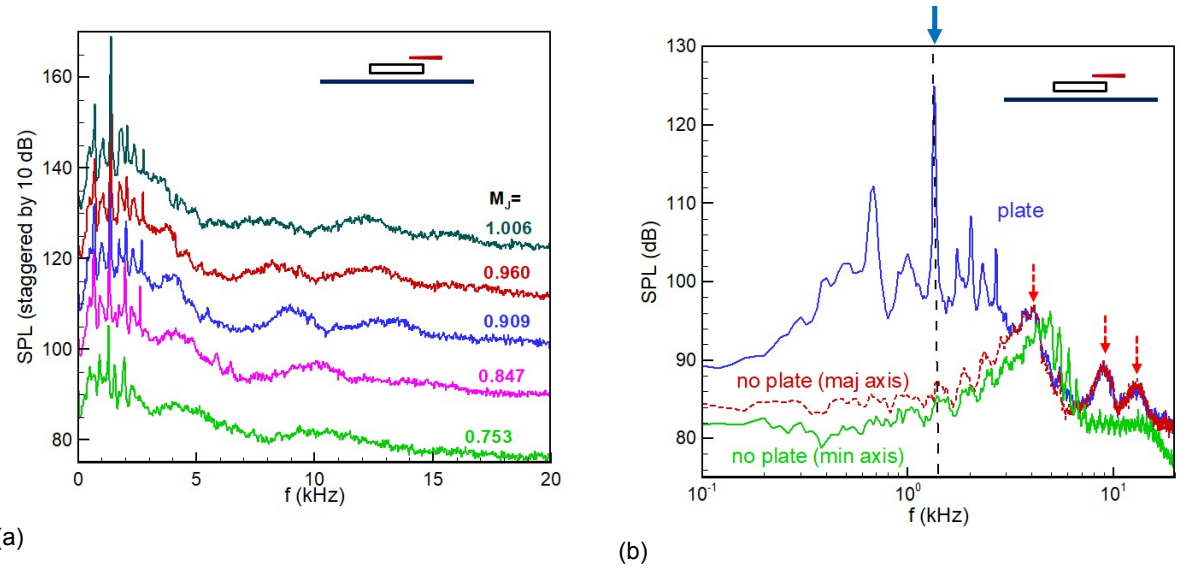

(a) (b)

Figure 16.—Pressure spectra for the 8:1 aspect ratio rectangular jet with a 12 by 24 in. plate underneath creating a resonant tone at 1375 Hz (plate surface 1.5 in. below long edge of nozzle and plate trailing edge 8.5 in. from exit). (a) Spectra for varying M_J with mic on long edge (y = 1.42, z = 0, x = 0.156), (b) spectra for M_J = 0.91 compared to corresponding no-plate data (log scale for abscissa).

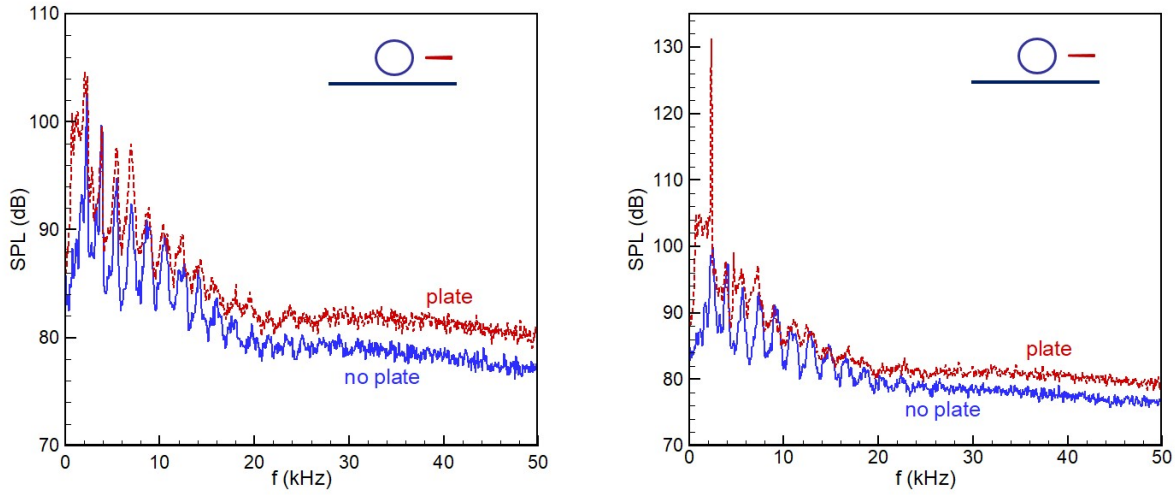

(a) (b)

Figure 17.—Pressure spectra for the SMC nozzle with a 6 by 8.5 in. plate underneath (plate surface 1.5 in. below jet axis and plate trailing edge 6 in. from exit); mic at x = 0.2 and r = 0.75. (a) At M_J = 0.91, the amplitudes increase across the frequency range but no resonance. (b) At M_J = 0.87, there is a resonance emitting a tone at 2360 Hz.

During the current explorations, a similar resonance phenomenon due to jet-surface interaction was encountered with the SMC nozzle. A clearer connection of the trapped wave spectral peaks with the resonant tones emerged from the corresponding data. First, Figure 17(a) shows that the presence of a plate near this nozzle amplifies the trapped wave spectral peaks. (This is in addition to producing low-frequency noise at <2 kHz presumably representing 'scrubbing noise'.) The broadband levels overall are also increased. While the data in Figure 17(a) is for M_J = 0.91, a slight decrease in M_J for the exact same hardware configuration yielded a sharp resonant tone, as shown in Figure 17(b). The geometric conditions and the details of the tones with the round nozzle remain to be explored further. However, it is clear that in this case the tone has locked on to the first trapped wave spectral peak seen otherwise without the presence of the plate.

Conclusions

Near the nozzle exit and around the edge of high-speed jets unsteady pressure fluctuations are observed that manifest as a series of peaks in the spectrum. These are apparently the footprints of 'trapped waves' within the potential core of the jet as revealed by recent research based on LES data mining as well as analytical studies. In this experimental study the characteristics of the spectral peaks are explored for a set of round nozzles of different diameters as well as a set of rectangular nozzles of different aspect ratios. In all cases, the frequency of the spectral peaks is found to decrease with increasing jet Mach number. For the round nozzles it is shown that the spectral peaks remain unaffected by the exit BL state and thickness. The frequencies are found to scale on the jet diameter. The Strouhal numbers based on the diameter for all nozzles are found to follow distinct branches of a family of curves when plotted as a function of M_J. This provides an engineering correlation for prediction of the frequencies. Curve-fit equations are provided for this purpose for the four most dominant spectral peaks.

With the rectangular nozzles the trapped wave spectral peaks are also observed. However, the frequencies of the peaks depend on the observation location. More tightly packed spectral peaks occur on

the short edge while the peaks are dispersed on the long edge. The ratio of the frequencies of the peaks on the short and long edge is found to be close to the aspect ratio of the nozzle.

For the 8:1 rectangular nozzle as well as the round SMC nozzle, the interaction of the jet with a surface nearby sometimes leads to resonant tones. The limited study carried out so far shows that the tone frequency for the round nozzle locks on to the first (lowest) trapped wave spectral peak. For the rectangular nozzle the resonance occurs when the plate is parallel to the long edge and the tone frequency appears to coincide with one of the trapped wave spectral peaks seen on the short edge. Even when there is no resonance the presence of a surface can amplify the peaks. Further explorations of the jet-surface interaction as well as the flow field characteristics related to the trapped waves are planned for the future.

References

1. Towne, A., Cavalieri, A.V.G., Jordan, P. Colonius, T., Schmidt, O., Jaunet, V. and Brès, G.A., "Acoustic resonance in the potential core of subsonic jets," *J. Fluid Mech*., vol. 825, pp. 1113–1152, doi:10.1017/jfm.2017.346, 2017.
2. Suzuki, T. and Colonius, T., "Instability waves in a subsonic round jet detected using a near-field phased microphone array," *J. Fluid Mech*., vol. 565, 197–226, 2006.
3. Zaman, K.B.M.Q., Fagan, A.F., Bridges, J.E., and Brown, C.A., 2015, "An experimental investigation of resonant interaction of a rectangular jet with a flat plate," *J. Fluid Mech*., vol. 779, pp. 751–775. doi:10.1017/jfm.2015.453, 2015.
4. Zaman, K.B.M.Q., "Exit Boundary Layer Data for a Round Convergent Nozzle in Support of Numerical Simulation Efforts," NASA/TM—2019-220242, July 2019.
5. Zaman, K.B.M.Q., "Flow-Field Surveys For Rectangular Nozzles," NASA/TM—2012-217410 (with electronic data files), April, 2012.
6. Tam, C. and Chandramouli, S., "Jet-plate interaction tones relevant to over-the-wing engine mount concept," AIAA Paper 2019-2430, AIAA/CEAS Aeroacoustics Conference, May 20–23, 2019, Delft, Netherlands, 2019.